

# Accelerating image reconstruction for low-dose X-ray CT and MRI

Jeffrey A. Fessler

EECS Dept., BME Dept., Dept. of Radiology  
University of Michigan

`web.eecs.umich.edu/~fessler`



JHU BME Department

09 Mar. 2015

# Disclosure

- Research support from GE Healthcare
- Supported in part by NIH grants R01 HL-098686, P01 CA-87634, U01 EB018753
- Equipment support from Intel Corporation

# Credits

## Current (CT) students / post-docs

- Donghwan Kim
- Jungkuk Kim
- Madison McGaffin
- Hung Nien
- Brian Gonzalez

## Current (MR) students

- Matt Muckley
- Hao Sun
- Sydney Williams
- Gopal Nataraj

## GE collaborators

- Bruno De Man
- Jiang Hsieh
- Jean-Baptiste Thibault

## CT collaborators

- Mitch Goodsitt, UM
- Ella Kazerooni, UM
- Neal Clinthorne, UM

## Former PhD students (who did/do CT)

- Sathish Ramani
- Stephen Schmitt
- Jang Hwan Cho
- Se Young Chun
- Yong Long, GE GRC
- Wonseok Huh, Bain & Company
- Hugo Shi, Continuum Analytics
- Joonki Noh, Emory
- Somesh Srivastava, GE HC
- Rongping Zeng, FDA
- Yingying, Zhang-O'Connor, RGM Advisors
- Matthew Jacobson, Xoran
- Sangtae Ahn, GE GRC
- Idris Elbakri, CancerCare / Univ. of Manitoba
- Saowapak Sotthivirat, NSTDA Thailand
- Web Stayman, JHU
- Feng Yu, Univ. Bristol
- Mehmet Yavuz, Qualcomm
- Hakan Erdoğan, Sabanci University

# Statistical image reconstruction: a CT revolution

- A picture is worth 1000 words
- (and perhaps several 1000 seconds of computation?)



Thin-slice FBP

Seconds



ASIR

A bit longer



Statistical

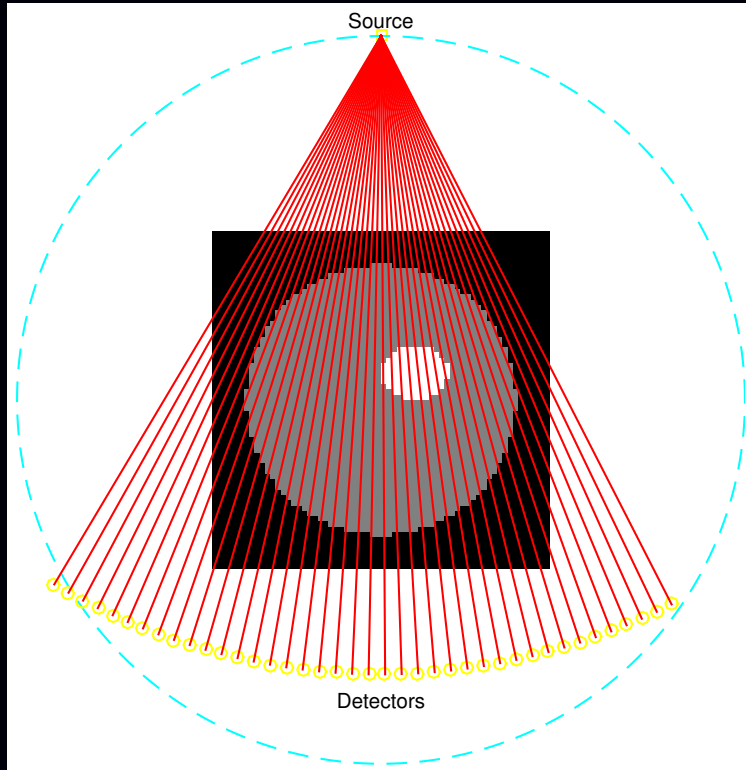
Much longer

(Same sinogram, so all at same **dose**)

# Outline

- **Model-based image reconstruction**
  - Low-dose X-ray CT
  - MRI
- **Accelerating low-dose X-ray CT image reconstruction**
  - Optimized first-order methods  
Donghwan Kim, JF; ArXiv 2014 Math. Prog., in review; ICIP 2015, submitted
  - Ordered-subsets + momentum  
Donghwan Kim, Sathish Ramani, JF; IEEE T-MI, Jan. 2015.
  - Distributed block-separable ordered subsets  
Donghwan Kim, JF; Fully 3D, 2015, to appear
  - Duality-based approach using GPU  
Madison G McGaffin, JF; Fully 3D, 2015, to appear
- **Accelerating model-based MR image reconstruction**
  - BARISTA (B1-based, adaptive restart, iterative soft thresholding algorithm)  
M. J. Muckley, D. C. Noll, JF; IEEE T-MI, Feb. 2015.

# X-ray CT scans



$$\begin{bmatrix} \text{yellow squares} \\ \vdots \\ \text{yellow squares} \end{bmatrix} = \begin{bmatrix} \text{orange grid} \\ \vdots \\ \text{orange grid} \end{bmatrix} \begin{bmatrix} \text{blue squares} \end{bmatrix} + \begin{bmatrix} \text{green squares} \\ \vdots \\ \text{green squares} \end{bmatrix}$$

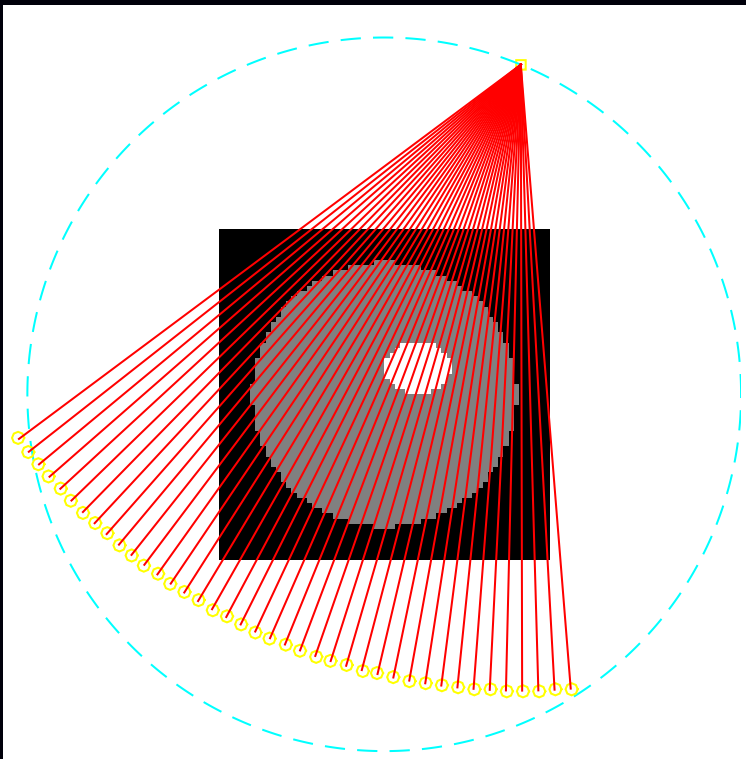
$y = Ax + \epsilon$

$y$ : measured data (sinogram)

$A$ : system matrix

$x$ : unknown image (attenuation map)

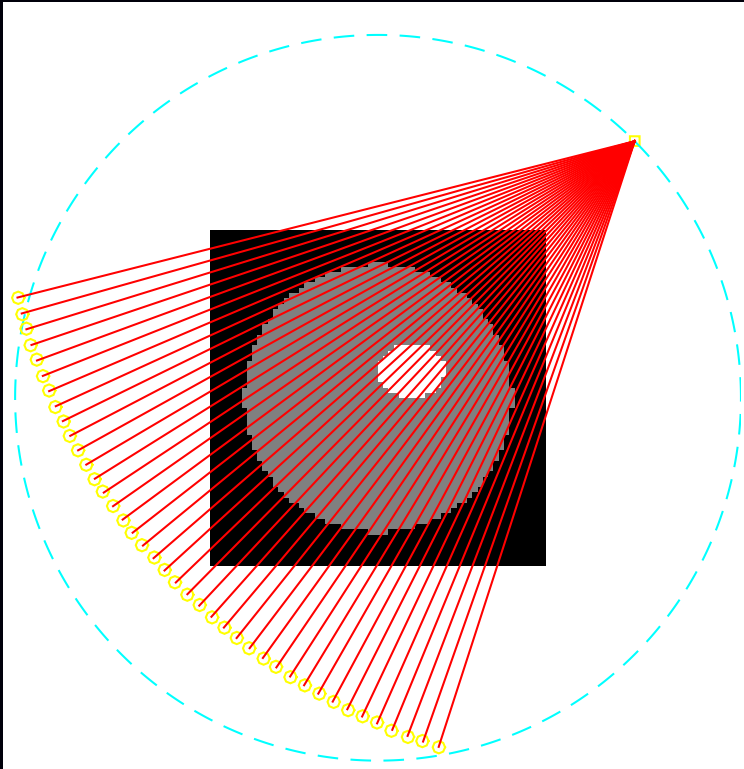
# X-ray CT scans



$$\begin{bmatrix} \text{yellow squares} \\ \vdots \\ \text{yellow squares} \end{bmatrix} = \begin{bmatrix} \text{orange squares} \\ \vdots \\ \text{orange squares} \end{bmatrix} \begin{bmatrix} \text{blue squares} \end{bmatrix} + \begin{bmatrix} \text{green squares} \\ \vdots \\ \text{green squares} \end{bmatrix}$$

$y = Ax + \varepsilon$

# X-ray CT scans

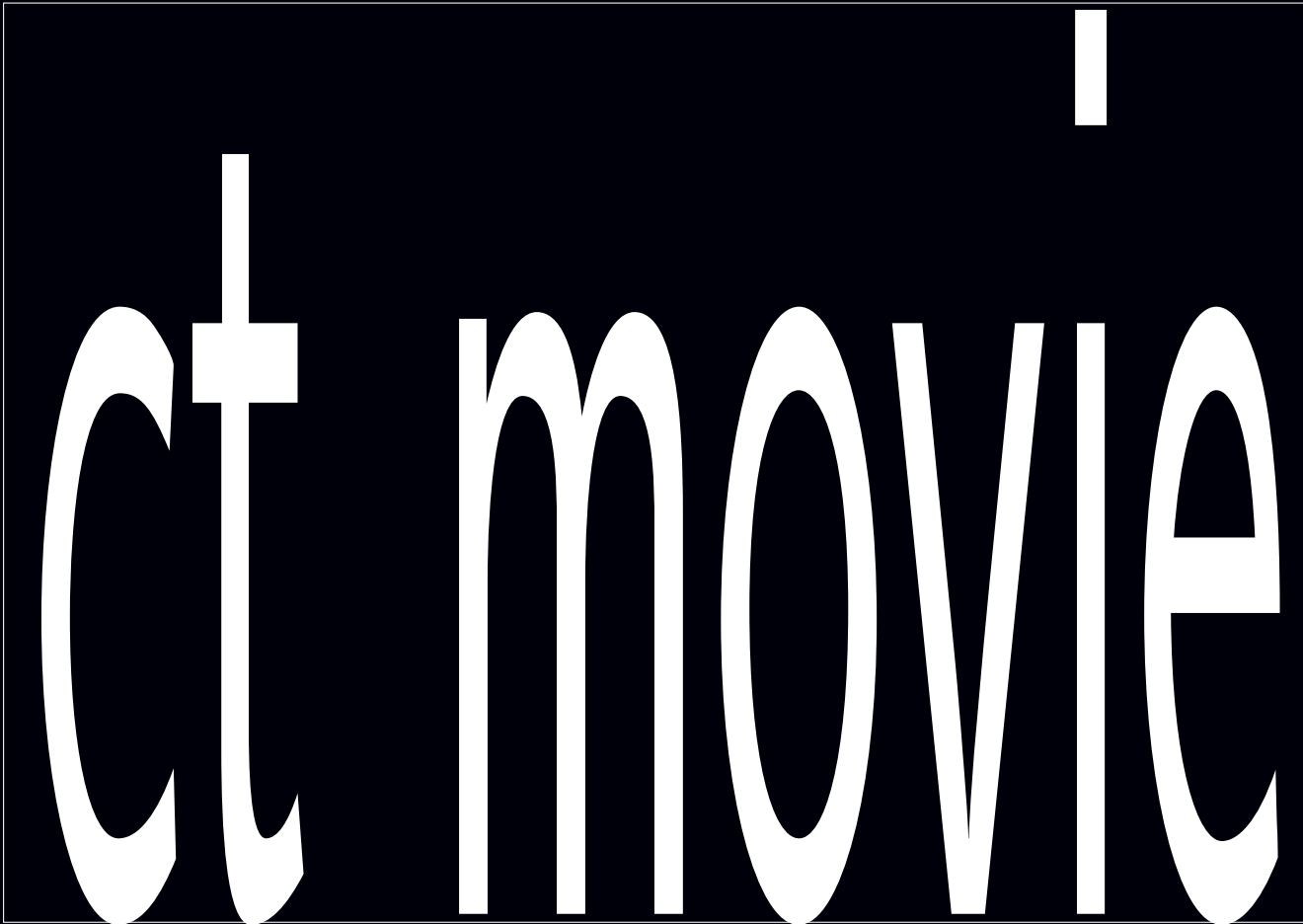


$$\begin{bmatrix} \text{yellow squares} \\ \vdots \\ \text{yellow squares} \end{bmatrix} = \begin{bmatrix} \text{orange grid} \\ \vdots \\ \text{orange grid} \end{bmatrix} \begin{bmatrix} \text{blue squares} \end{bmatrix} + \begin{bmatrix} \text{green squares} \\ \vdots \\ \text{green squares} \end{bmatrix}$$

$y = Ax + \epsilon$



## X-ray CT scans

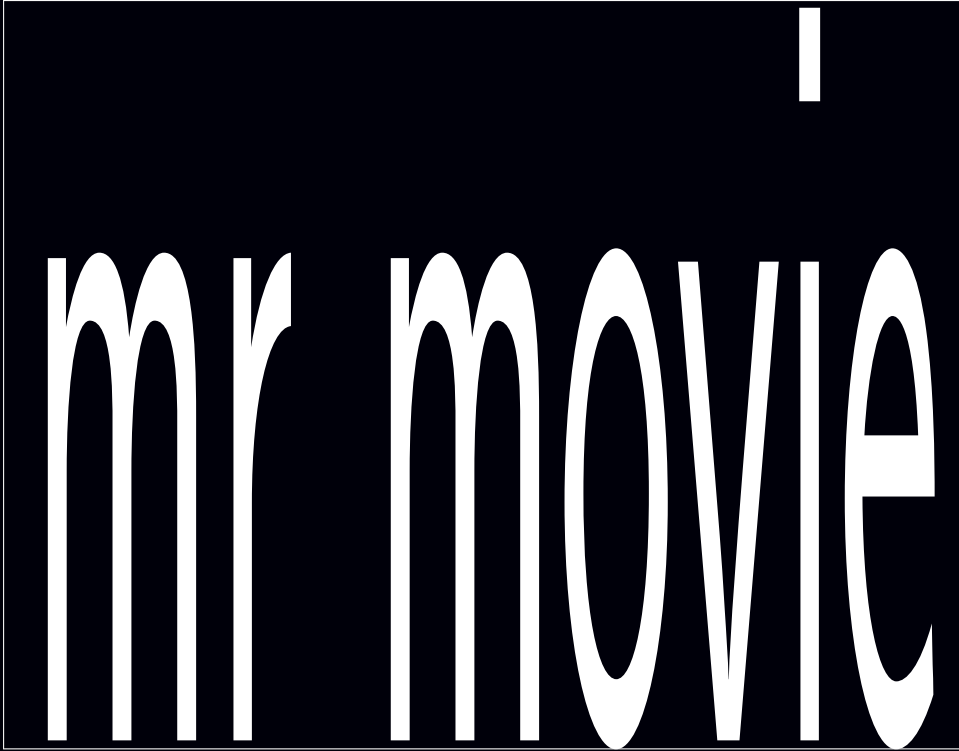


CT image reconstruction problem:  
Determine attenuation map  $x$  from sinogram data  $y$

Ignoring motion hereafter...

## MRI scans

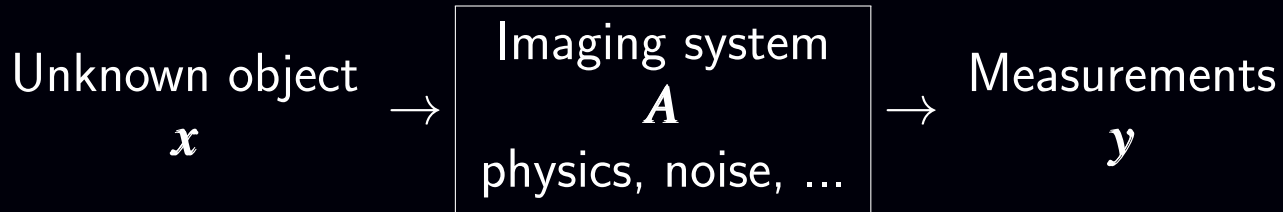
No moving parts to animate...



MR image reconstruction problem:

Determine magnetization image  $\mathbf{x}$  from k-space data  $\mathbf{y}$

# Inverse problems



How to reconstruct object  $x$  from data  $y$ ?

## Classical approach:

- analytical / direct / non-iterative
  - Filtered back-projection (FBP) for CT
  - Inverse FFT for MRI
- idealized description of the system
  - geometry / sampling
  - disregards noise and simplifies physics
- typically fast

## Contemporary approach:

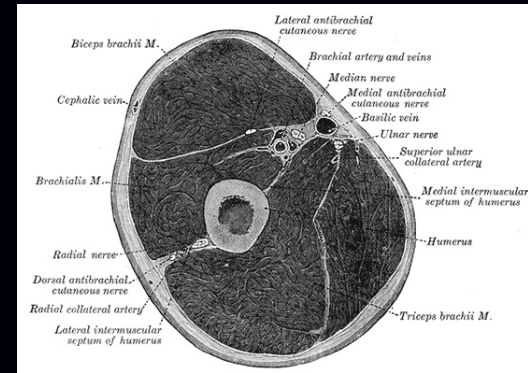
- model-based / statistical / iterative
- based on “reasonably accurate” models for physics and statistics
- usually much slower

# Why statistical/iterative methods for CT?

- Accurate **physics** models
  - X-ray spectrum, beam-hardening, scatter, ...  
⇒ reduced artifacts? quantitative CT?
  - X-ray detector spatial response, focal spot size, ...  
⇒ improved spatial resolution?
  - detector spectral response (e.g., photon-counting detectors)  
⇒ improved contrast between distinct material types?
- Nonstandard **geometries**
  - transaxial truncation (wide patients)
  - long-object problem in helical CT
  - irregular sampling in “next-generation” geometries
  - coarse angular sampling in image-guidance applications
  - limited angular range (tomosynthesis)
  - “missing” data, e.g., bad pixels in flat-panel systems
- Appropriate models of (data dependent) measurement **statistics**
  - weighting reduces influence of photon-starved rays (*cf.* FBP)  
⇒ reducing image noise or X-ray **dose**

## and more...

- **Object** constraints / priors
  - nonnegativity
  - object support
  - piecewise smoothness
  - object sparsity (e.g., angiography)
  - sparsity in some basis
  - motion models
  - dynamic models
  - ...



Henry Gray, Anatomy of the Human Body, 1918, Fig. 413.

These constraints may help reduce image artifacts or noise or **dose**.

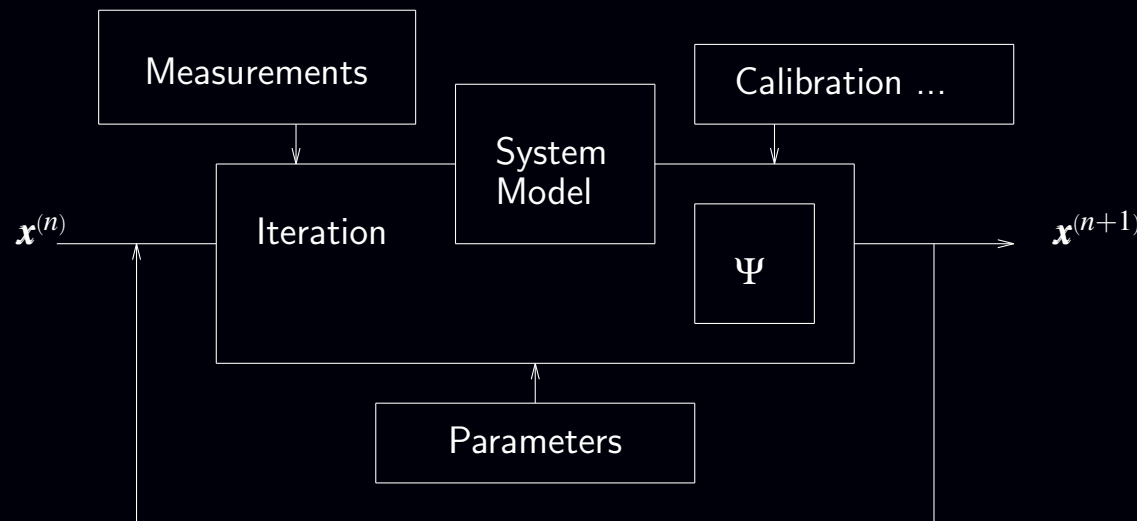
## Disadvantages?

- Computation **time** (super computer)
- Must reconstruct entire FOV
- Complexity of models and software
- Algorithm **nonlinearities**
  - Difficult to analyze resolution/noise properties (cf. FBP)
  - Tuning parameters
  - Challenging to characterize performance / assess image quality

# Statistical image reconstruction overview

- Object model
- Physics/system model
- Statistical model
- Cost function  $\Psi = \text{log-likelihood} + \text{regularization}$
- Iterative algorithm for minimization

“Find the image  $\hat{x}$  that best fits the measured data  $y$  according to the physics model, the measurement statistics model and prior information about the object”



- Repeatedly revisiting the sinogram data can use measurement statistics fully
- Repeatedly updating the image can exploit object properties
- $\therefore$  greatest potential **dose reduction**, but repetition is expensive...

## Sub-mSv example

3D helical X-ray CT scan of abdomen/pelvis:

100 kVp, 25-38 mA, 0.4 second rotation, 0.625 mm slice, 0.6 mSv.



FBP



ASIR



Statistical

## MBIR example: Routine chest CT

Helical chest CT study with dose = 0.09 mSv.

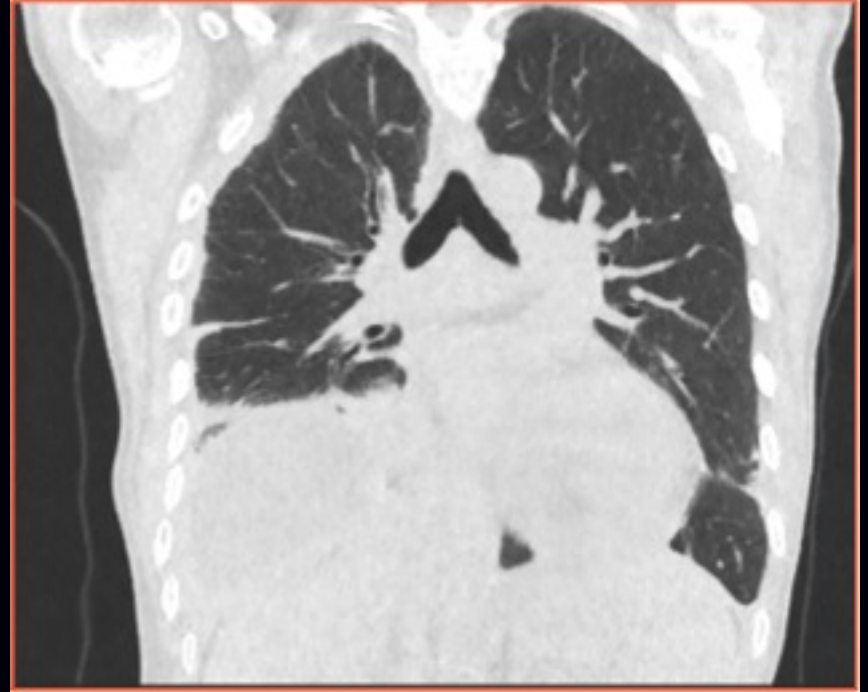
Typical CXR effective dose is about 0.06 mSv.

Source: Health Physics Society.

<http://www.hps.org/publicinformation/ate/q2372.html>



FBP



MBIR

Veo (MBIR) images courtesy of Jiang Hsieh, GE Healthcare



# History: Statistical reconstruction for PET

- Iterative method for emission tomography (Kuhl, 1963)
- FBP for PET (Chesler, 1971)
- Weighted least squares for 3D SPECT (Goitein, NIM, 1972)
- Richardson/Lucy iteration for image restoration (1972, 1974)
- Poisson likelihood (emission) (Rockmore and Macovski, TNS, 1976)
- Expectation-maximization (EM) algorithm (Shepp and Vardi, TMI, 1982)
- Regularized (aka Bayesian) Poisson emission reconstruction (Geman and McClure, ASA, 1985)
- Ordered-subsets EM (OSEM) algorithm (Hudson and Larkin, TMI, 1994)
- Commercial release of OSEM for PET scanners circa 1997

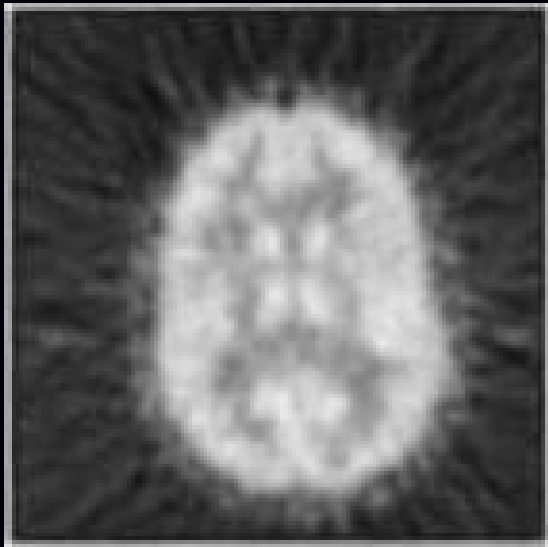
Today, most (all?) commercial PET systems include *unregularized* OSEM.

15 years between key EM paper (1982) and commercial adoption (1997)  
(25 years if you count the R/L paper in 1972 which is the same as EM)

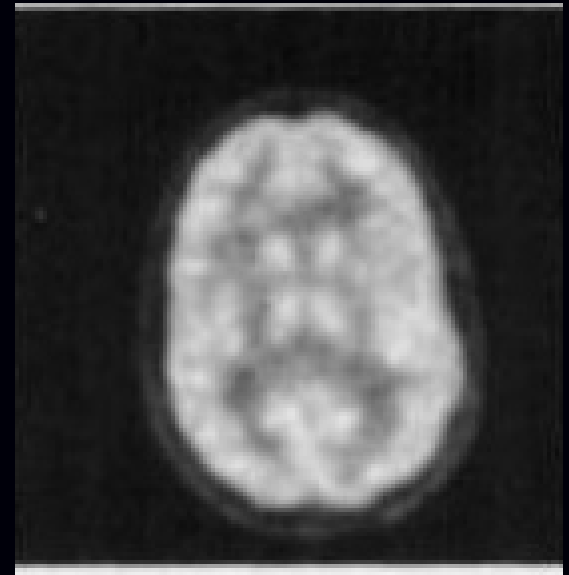
## Key factors in PET

- OS algorithm accelerated convergence by order of magnitude
- Computers got faster (but problem size grew too)
- Key clinical validation papers?
- Key numerical observer studies?
- Nuclear medicine physicians grew accustomed to appearance of images reconstructed using statistical methods

FBP:

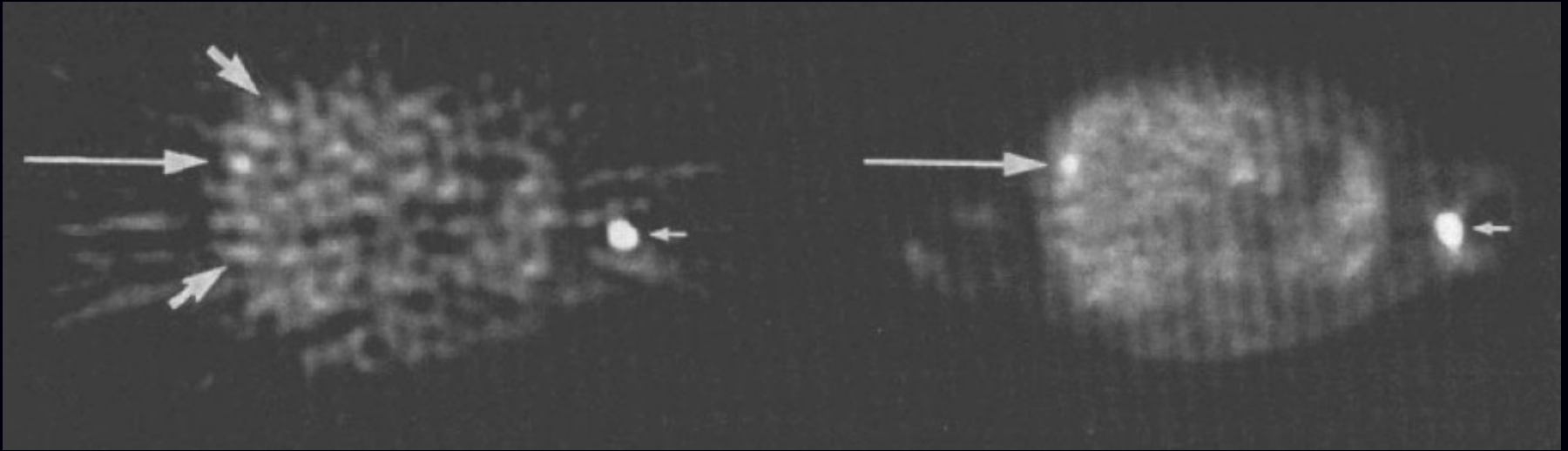


ML-EM:



Llacer *et al.*, 1993

## Whole-body PET example



FBP

ML-OSEM

Meikle *et al.*, 1994

Key factor in PET: modeling measurement statistics

# History: Statistical reconstruction for CT\*

- Iterative method for X-ray CT (Hounsfield, 1968)
- ART for tomography (Gordon, Bender, Herman, JTB, 1970)
- ...
- Roughness regularized LS for tomography (Kashyap & Mittal, 1975)
- Poisson likelihood (transmission) (Rockmore and Macovski, TNS, 1977)
- EM algorithm for Poisson transmission (Lange and Carson, JCAT, 1984)
- Iterative coordinate descent (ICD) (Sauer and Bouman, T-SP, 1993)
- Ordered-subsets algorithms (Manglos *et al.*, PMB 1995)  
(Kamphuis & Beekman, T-MI, 1998)  
(Erdoğan & Fessler, PMB, 1999)
- ...
- Commercial introduction of ICD for CT scanners circa 2010
- FDA 510(k) clearance of Veo Sep. 2011
- First Veo installation in USA (at UM) Jan. 2012

(\* numerous omissions, including many denoising methods)

# Statistical image reconstruction for low-dose CT

Optimization problem formulation:

$$\hat{\mathbf{x}} = \underbrace{\arg \min_{\mathbf{x} \geq \mathbf{0}}}_{\substack{\text{optimization} \\ \text{algorithm}}} \underbrace{\Psi(\mathbf{x})}_{\substack{\text{cost} \\ \text{function}}} \triangleq \underbrace{\frac{1}{2} \|\mathbf{y} - \mathbf{A}\mathbf{x}\|_{\mathbf{W}}^2}_{\substack{\text{data-fit term} \\ \text{physics \& statistics}}} + \underbrace{\beta \sum_{j=1}^N \sum_{k \in \mathcal{N}_j} \psi(x_j - x_k)}_{\substack{\text{regularizer} \\ \text{prior models}}}$$

$\mathbf{y}$  : measured data (sinogram)

$\mathbf{A}$  : system matrix (physics / geometry)

$\mathbf{W}$  : weighting matrix (statistics)

$\mathbf{x}$  : unknown image (attenuation map)

$\psi$  : edge-preserving potential function (piece-wise smoothness / sparse gradients)

Optimization challenges:

- large problem size:  $\mathbf{x} \in \mathbb{R}^{512 \times 512 \times 600}$ ,  $\mathbf{y} \in \mathbb{R}^{888 \times 64 \times 7000}$
- $\mathbf{A}$  is sparse but still too large to store; compute  $\mathbf{A}\mathbf{x}$  on-the-fly
- $\mathbf{W}$  has enormous dynamic range (1 to  $\exp(-9) \approx 1.2 \cdot 10^{-4}$ )
- Gram matrix  $\mathbf{A}'\mathbf{W}\mathbf{A}$  highly shift variant
- $\Psi$  is non-quadratic but convex (and often smooth)

# Optimization algorithms for X-ray CT

# Classical gradient descent (GD)

Assumptions:

- $\Psi$  is convex (need not be strictly convex)
- $\Psi$  has non-empty set of global minimizers  
 $\hat{\mathbf{x}} \in \mathcal{X}^* = \{\mathbf{x}^{(*)} \in \mathbb{R}^N : \Psi(\mathbf{x}^{(*)}) \leq \Psi(\mathbf{x}), \forall \mathbf{x} \in \mathbb{R}^N\}$
- $\Psi$  is smooth (differentiable with  $L$ -Lipshitz gradient)  
 $\|\nabla \Psi(\mathbf{x}) - \nabla \Psi(\mathbf{z})\|_2 \leq L \|\mathbf{x} - \mathbf{z}\|_2, \quad \forall \mathbf{x}, \mathbf{z} \in \mathbb{R}^N$

Gradient descent (GD) with step size  $1/L$  ensures monotonic descent of  $\Psi$ :

$$\mathbf{x}^{(n+1)} = \mathbf{x}^{(n)} - \frac{1}{L} \nabla \Psi(\mathbf{x}^{(n)}).$$

Drori & Teboulle (2014) derive tightest “inaccuracy” bound:

$$\underbrace{\Psi(\mathbf{x}^{(n)}) - \Psi(\mathbf{x}^{(*)})}_{\text{inaccuracy}} \leq \frac{L \|\mathbf{x}^{(0)} - \mathbf{x}^{(*)}\|_2^2}{4n + 2}.$$

They construct a Huber-like function  $\Psi$  for which GD achieves that (tight) bound.

But  $O(1/n)$  rate is undesirably slow.

# Nesterov's fast gradient method (FGM1)

Nesterov (1983) iteration: Initialize:  $t_0 = 1, \mathbf{z}^{(0)} = \mathbf{x}^{(0)}$

$$\mathbf{z}^{(n+1)} = \mathbf{x}^{(n)} - \frac{1}{L} \nabla \Psi(\mathbf{x}^{(n)}) \quad (\text{usual GD update})$$

$$t_{n+1} = \frac{1}{2} \left( 1 + \sqrt{1 + 4t_n^2} \right) \quad (\text{magic momentum factors})$$

$$\mathbf{x}^{(n+1)} = \mathbf{z}^{(n+1)} + \frac{t_n - 1}{t_{n+1}} (\mathbf{z}^{(n+1)} - \mathbf{z}^{(n)}) \quad (\text{update with momentum}).$$

Reverts to GD if  $t_n = 1, \forall n$ .

Shown by Nesterov to be  $O(1/n^2)$  for “auxiliary” sequence:

$$\Psi(\mathbf{z}^{(n)}) - \Psi(\mathbf{x}^{(\star)}) \leq \frac{2L \|\mathbf{x}^{(0)} - \mathbf{x}^{(\star)}\|_2^2}{(n+1)^2}.$$

Nesterov constructed a function  $\Psi$  such that any first-order method achieves

$$\frac{\frac{3}{32}L \|\mathbf{x}^{(0)} - \mathbf{x}^{(\star)}\|_2^2}{(n+1)^2} \leq \Psi(\mathbf{x}^{(n)}) - \Psi(\mathbf{x}^{(\star)}).$$

Thus  $O(1/n^2)$  rate of FGM1 is optimal.

Donghwan Kim (2014) analyzed primary sequence:  $\Psi(\mathbf{x}^{(n)}) - \Psi(\mathbf{x}^{(\star)}) \leq \frac{2L \|\mathbf{x}^{(0)} - \mathbf{x}^{(\star)}\|_2^2}{(n+2)^2}.$



# Generalizing Nesterov's FGM

FGM1 is in the general class of first-order methods:

$$\mathbf{x}^{(n+1)} = \mathbf{x}^{(n)} - \frac{1}{L} \sum_{k=0}^n h_{n+1,k} \nabla \Psi(\mathbf{x}^{(k)})$$

where the step-size factors  $\{h_{n,k}\}$  are given by:

$$h_{n+1,k} = \begin{cases} \frac{t_n - 1}{t_{n+1}} h_{n,k}, & k = 0, \dots, n-2 \\ \frac{t_n - 1}{t_{n+1}} (h_{n,n-1} - 1), & k = n-1 \\ 1 + \frac{t_n - 1}{t_{n+1}}, & k = n. \end{cases}$$

$$\begin{bmatrix} 1 & 0 & 0 & 0 & 0 & 0 \\ 0 & 1.25 & 0 & 0 & 0 & 0 \\ 0 & 0.10 & 1.40 & 0 & 0 & 0 \\ 0 & 0.05 & 0.20 & 1.50 & 0 & 0 \\ 0 & 0.03 & 0.11 & 0.29 & 1.57 & 0 \\ 0 & 0.02 & 0.07 & 0.18 & 0.36 & 1.62 \end{bmatrix}$$

Note use of previous gradients  $\implies$  “momentum”

Is this the optimal choice for  $\{h_{n,k}\}$  ?

Can we do better than the constant 2 in worst-case convergence rate?

Drori & Teboulle (2014) numerically find  $\{h_{n,k}\}$  that are factor of two better.  
(Factors of two matter practically.)

# Optimized gradient method (OGM1)

New approach by optimizing  $\{h_{n,k}\}$  analytically (Donghwan Kim and JF; 2014, 2015):

Initialize:  $t_0 = 1, \mathbf{z}^{(0)} = \mathbf{x}^{(0)}$

$$\mathbf{z}^{(n+1)} = \mathbf{x}^{(n)} - \frac{1}{L} \nabla \Psi(\mathbf{x}^{(n)}) \quad (\text{usual GD update})$$

$$t_{n+1} = \frac{1}{2} \left( 1 + \sqrt{1 + 4t_n^2} \right) \quad (\text{momentum factors})$$

$$\mathbf{x}^{(n+1)} = \mathbf{z}^{(n+1)} + \frac{t_n - 1}{t_{n+1}} (\mathbf{z}^{(n+1)} - \mathbf{z}^{(n)}) + \underbrace{\frac{t_n}{t_{n+1}} (\mathbf{z}^{(n+1)} - \mathbf{x}^{(n)})}_{\text{new momentum}}.$$

Faster (worst-case) convergence by factor of 2:

$$\Psi(\mathbf{z}^{(n)}) - \Psi(\mathbf{x}^{(\star)}) \leq \frac{1L \|\mathbf{x}^{(0)} - \mathbf{x}^{(\star)}\|_2^2}{(n+1)^2}.$$

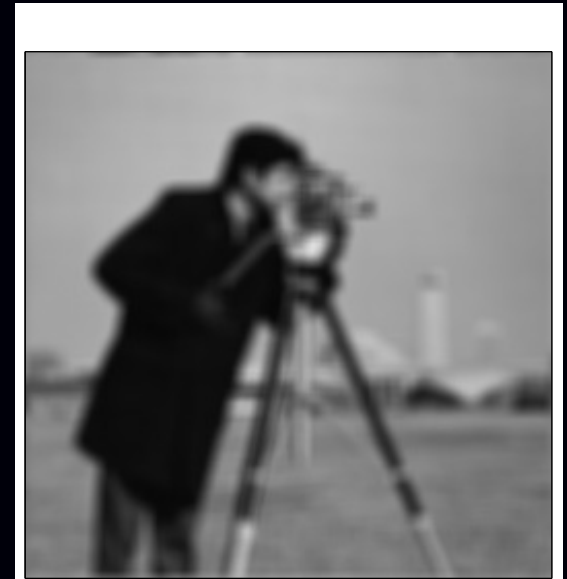
Recently (last week) found a Huber-like function for which OGM1 achieves that upper bound, inspired by work of Taylor *et al.* (2015).

# Example: Image restoration (!?)

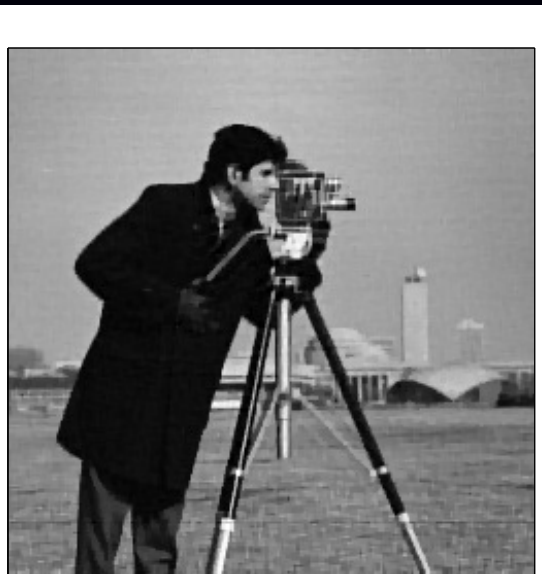
True  $x$ :



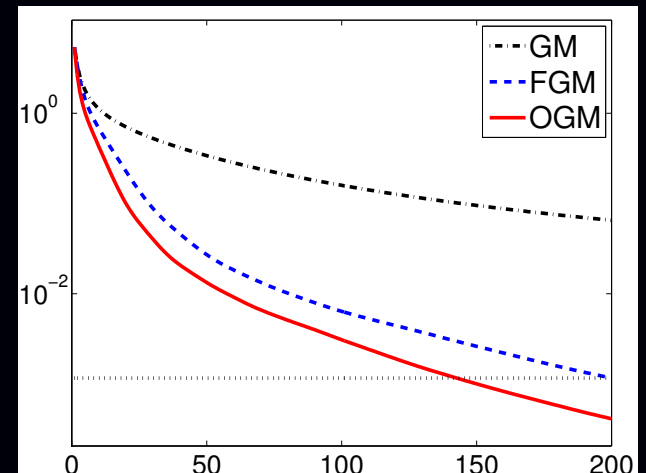
Blurred  $y$ :



Restored  
 $\hat{x}$



Rate:  
 $\Psi(x^{(n)}) - \Psi(\hat{x})$   
vs iteration  $n$



# Ordered subsets version of OGM1

For further acceleration, combine OGM with ordered subsets (OS)

$$\Psi(\mathbf{x}) = \sum_{m=1}^M \Psi_m(\mathbf{x}), \quad \Psi_m(\mathbf{x}) \triangleq \underbrace{\frac{1}{2} \|\mathbf{y}_m - \mathbf{A}_m \mathbf{x}\|_{\mathbf{W}_m}^2}_{1/M \text{th of measurements}} + \frac{1}{M} R(\mathbf{x})$$

Initialize:  $t_0 = 1$ ,  $\mathbf{z}^{(0)} = \mathbf{x}^{(0)}$

for  $n = 0, 1, \dots$  (iteration)

for  $m = 1, \dots, M$  (subset)

$k = nM + m$  (subiteration)

$$\mathbf{z}^{k+1} = [\mathbf{x}^k - \mathbf{D}M \nabla \Psi_m(\mathbf{x}^k)]_+ \quad (\text{typical OS-SQS})$$

$$t_{k+1} = \frac{1}{2} \left( 1 + \sqrt{1 + 4t_k^2} \right)$$

$$\mathbf{x}^{k+1} = \mathbf{z}^{k+1} + \frac{t_k - 1}{t_{k+1}} (\mathbf{z}^{k+1} - \mathbf{z}^k) + \frac{t_k}{t_{k+1}} (\mathbf{z}^{k+1} - \mathbf{x}^k) \quad (\text{momentum})$$

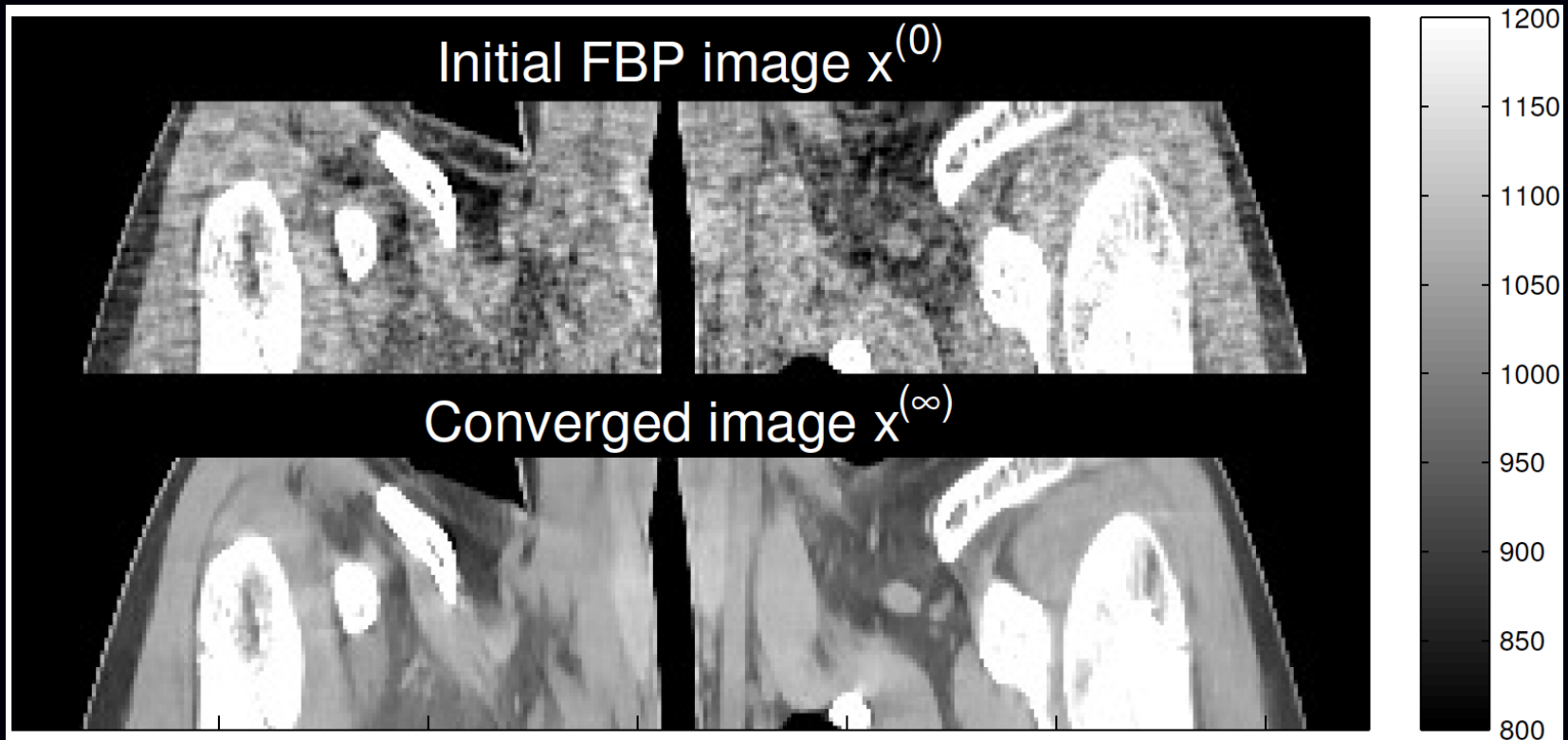
Approximate convergence rate for  $\Psi$ :  $O\left(\frac{1}{n^2 M^2}\right)$

(Donghwan Kim and JF; CT 2014)

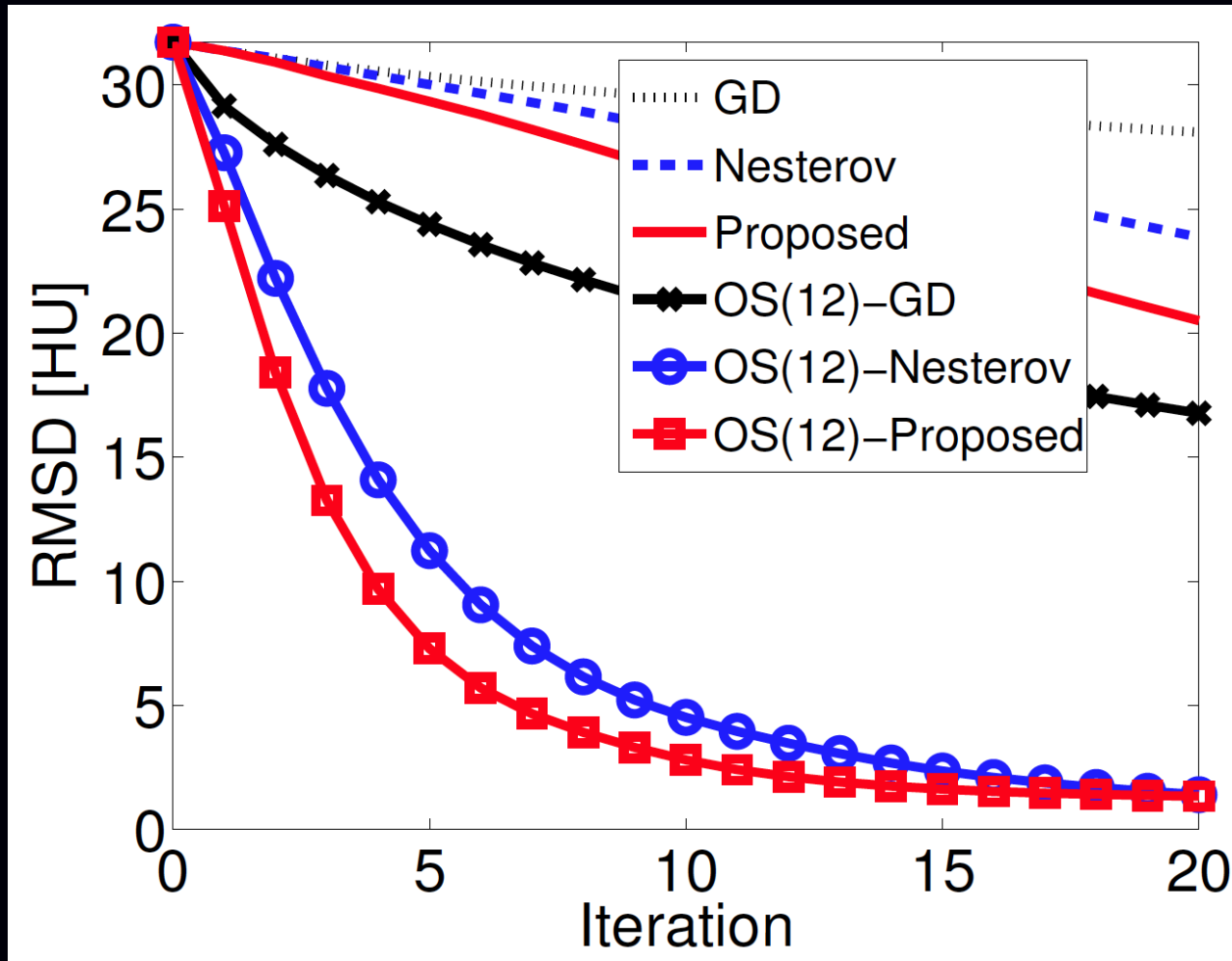
Now fast enough to show an X-ray CT example...

## OS+OGM results: data

- 3D cone-beam helical X-ray CT scan
- pitch 0.5
- image  $\mathbf{x}$ :  $512 \times 512 \times 109$  with 70 cm FOV and 0.625 mm slices
- sinogram :  $\mathbf{y}$  888 detectors  $\times$  32 rows  $\times$  7146 views

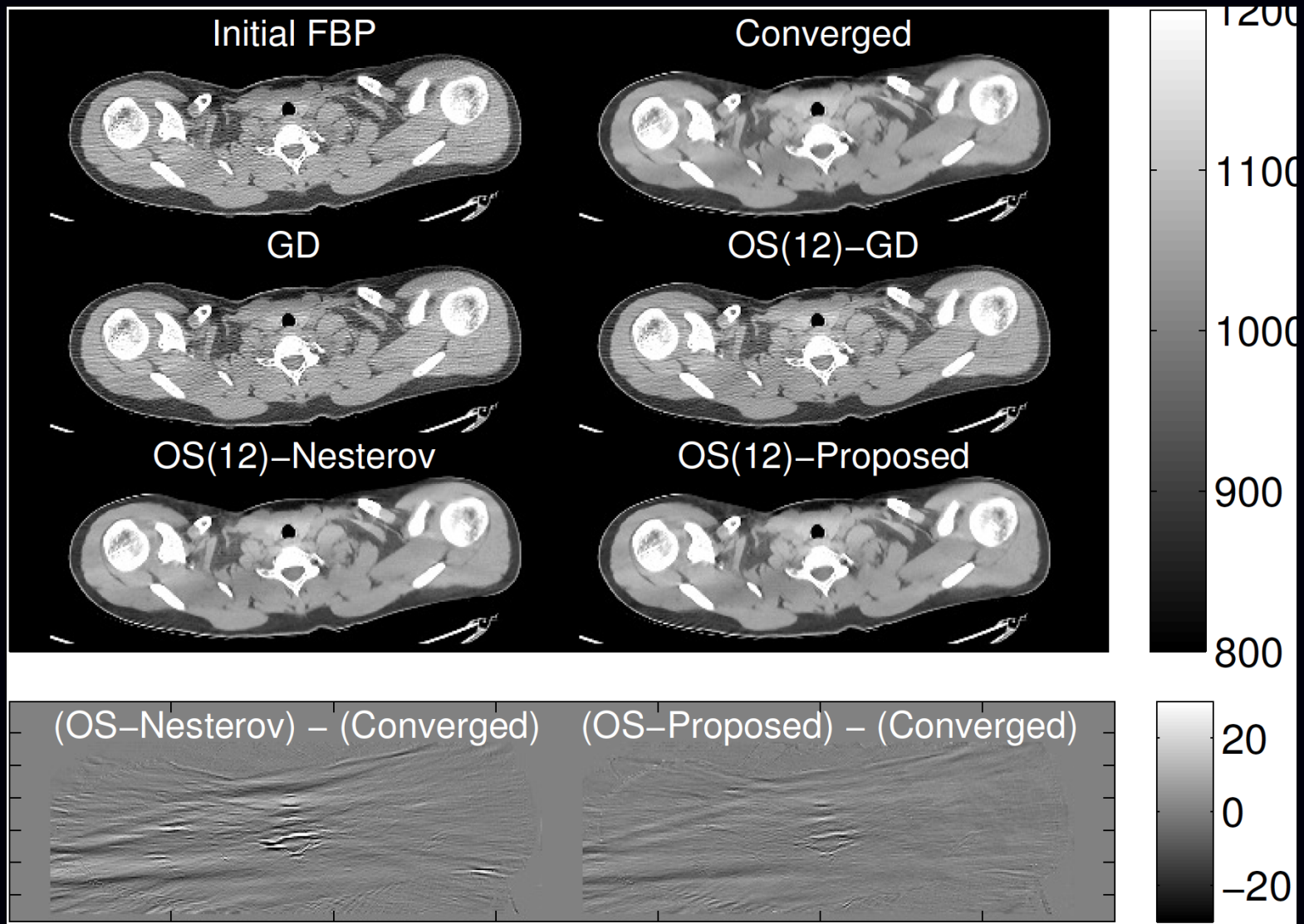


## OS+OGM results: convergence rate



Root mean square difference (RMSD) between  $\mathbf{x}^{(n)}$  and  $\mathbf{x}^{(\infty)}$  over ROI (in HU), versus iteration. (Compute time per iteration very similar.)

## OS+OGM results: images



At iteration 10 with  $M = 12$  subsets.

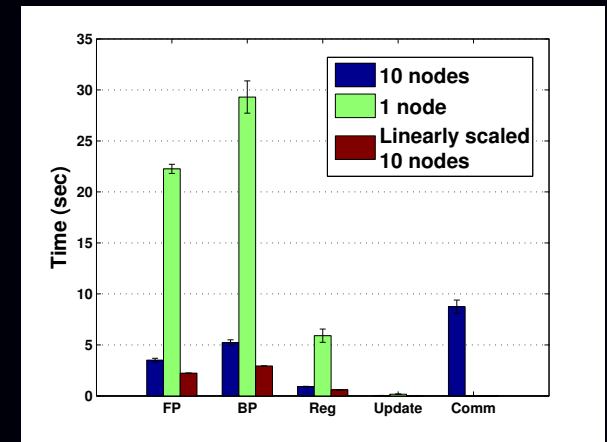
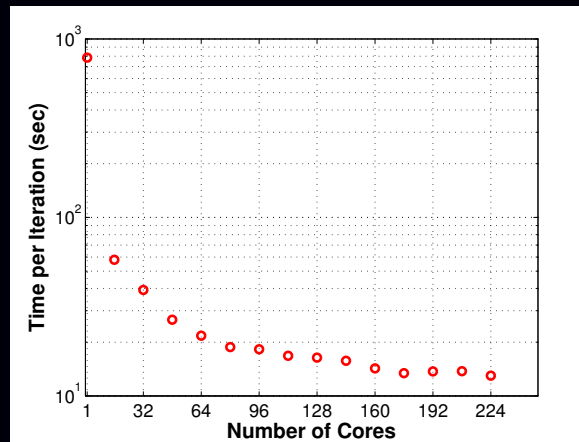
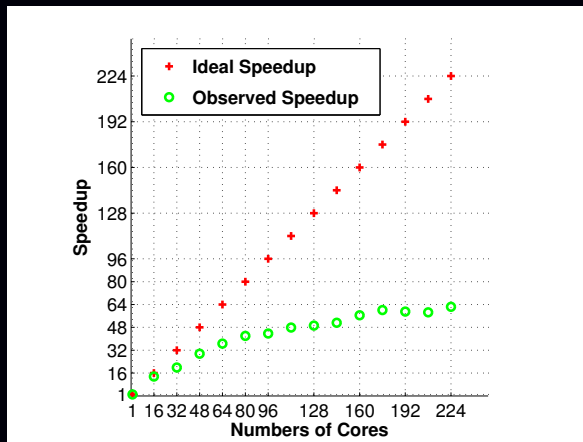
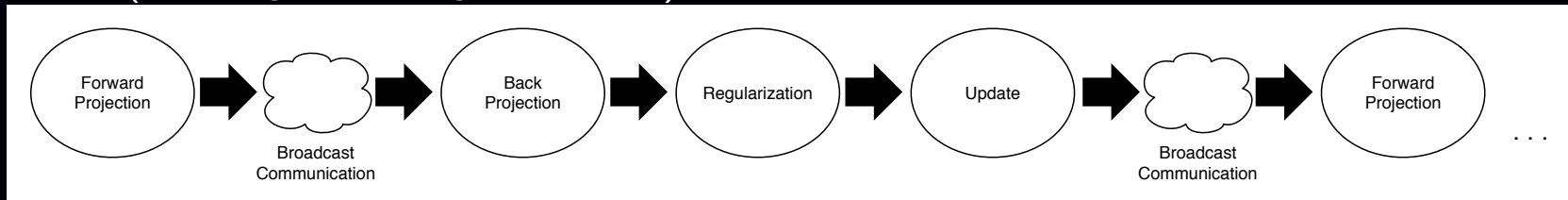
## Towards parallel computing



# Amazon Cloud version of OS+OGM

Distribute long object (320 useful slices) into (overlapping) slabs (128 slices each) across 5 separate clusters, each with 10 nodes having 16 cores.

Use MPI (message passing interface) for within-cluster communication:



Rosen *et al.* (Fully 3D, 2013)

- Overlapping slabs is inefficient
- Communication time (within cluster, after *every subset*) is serious bottleneck

# Block-separable surrogates for distributed reconstruction

Conventional OS approach uses a (voxel) separable quadratic surrogate (SQS):

$$\begin{aligned}\Psi(\mathbf{x}) - \Psi(\mathbf{x}^{(n)}) &\leq \nabla \Psi(\mathbf{x}^{(n)}) (\mathbf{x} - \mathbf{x}^{(n)}) + \frac{1}{2} (\mathbf{x} - \mathbf{x}^{(n)})' \mathbf{D} (\mathbf{x} - \mathbf{x}^{(n)}) \\ &= \sum_{j=1}^N \frac{\partial}{\partial x_j} \Psi(\mathbf{x}^{(n)}) (x_j - x_j^{(n)}) + \frac{1}{2} d_j (x_j - x_j^{(n)})^2,\end{aligned}$$

where diagonal matrix  $\mathbf{D}$  majorizes the Hessian of  $\Psi$ :  $\nabla^2 \Psi(\mathbf{x}) \leq \mathbf{D}$ .

Distributed computing alternative: derive slab-separable surrogate instead:

$$\Psi(\mathbf{x}) - \Psi(\mathbf{x}^{(n)}) \leq \sum_{b=1}^B \Psi_b(\mathbf{x}_b), \quad \Psi_b(\mathbf{x}_b) \triangleq \nabla_{\mathbf{x}_b} \Psi(\mathbf{x}^{(n)}) (\mathbf{x}_b - \mathbf{x}_b^{(n)}) + \frac{1}{2} (\mathbf{x}_b - \mathbf{x}_b^{(n)})' \mathbf{H}_b (\mathbf{x}_b - \mathbf{x}_b^{(n)}),$$

where *block* diagonal matrix  $\mathbf{H} = \text{diag}\{\mathbf{H}_1, \dots, \mathbf{H}_B\}$  majorizes the Hessian of  $\Psi$ .

$$\mathbf{H}_b \triangleq \mathbf{A}_b' \mathbf{W} \Lambda_b \mathbf{A}_b, \quad \Lambda_b \triangleq \text{diag}\{\mathbf{A}_b \mathbf{1} \odot \mathbf{A}_b \mathbf{1}_b\}$$

Updates parallelizable across blocks (slabs): (Donghwan Kim and JF; Fully 3D, 2015)

$$\mathbf{x}_b^{(n+1)} \triangleq \arg \min_{\mathbf{x}_b \succeq \mathbf{0}} \Psi_b(\mathbf{x}_b).$$

Reduces communication. (Apply favorite optimization method within slab.)

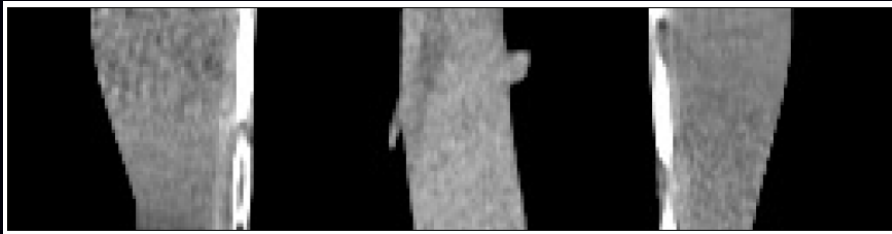
# Block-separable surrogate (BSS) OS+OGM

- 1: Initialize  $\tilde{\mathbf{x}}^{(0)}$  by FBP, and compute  $\mathbf{D}$ .
- 2: Distribute image  $\tilde{\mathbf{x}}^{(0)}$  and data  $\mathbf{y}$  into  $B$  nodes.
- 3: **for**  $n = 0, 1, \dots$
- 4: Minimize  $\phi_{\text{BSS}}(\mathbf{x}; \tilde{\mathbf{x}}^{(n)})$  using  $L$  sub-iterations of OS-SQS-mom.
  - 1) Initialize  $\mathbf{x}^{(0)} = \mathbf{z}^{(0)}$  by  $\tilde{\mathbf{x}}^{(n)}$ , and  $t^{(0)} = 1$ .
  - 2) **for**  $l = 0, 1, \dots, L - 1$
  - 3)  $m = l \bmod M$
  - 4)  $t^{(l+1)} = \frac{1}{2} \left( 1 + \sqrt{1 + 4 [t^{(l)}]^2} \right)$
  - 5) **for**  $b = 1, \dots, B$  **simultaneously**
  - 6)  $\mathbf{g}_{m,b}^{(l)} = M \nabla_b \phi_{\text{BSS},m}(\mathbf{z}^{(\frac{l}{M})}; \mathbf{z}^{(0)})$  [subset gradient]
  - 7)  $\mathbf{x}_b^{(\frac{l+1}{M})} = \left[ \mathbf{z}_b^{(\frac{l}{M})} - \mathbf{D}_b^{-1} \mathbf{g}_{m,b}^{(l)} \right]_+$  [OS-SQS update]
  - 8)  $\mathbf{z}_b^{(\frac{l+1}{M})} = \mathbf{x}_b^{(\frac{l+1}{M})} + \frac{t^{(l)} - 1}{t^{(l+1)}} \left( \mathbf{x}_b^{(\frac{l+1}{M})} - \mathbf{x}_b^{(\frac{l}{M})} \right)$  [momentum]
  - 9) **end for**
  - 10) **end for**
  - 11)  $\tilde{\mathbf{x}}^{(n+1)} = \mathbf{x}^{(\frac{L}{M})}$
- 5: **Communicate**  $\tilde{\mathbf{x}}^{(n+1)}$ .
- 6: **end for**

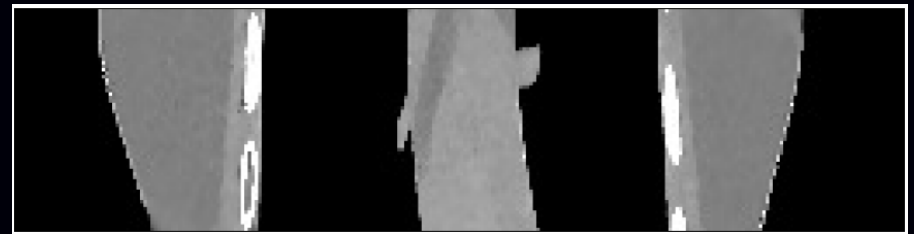
## BSS OS+OGM: data

- $256 \times 256 \times 160$  XCAT phantom (Segars *et al.*, 2008)
- Simulated helical CT,  $444 \times 32 \times 492$
- $M = 12$  subsets,  $B = 10$  blocks,  $L = 5$  inner iterations
- Matlab emulation

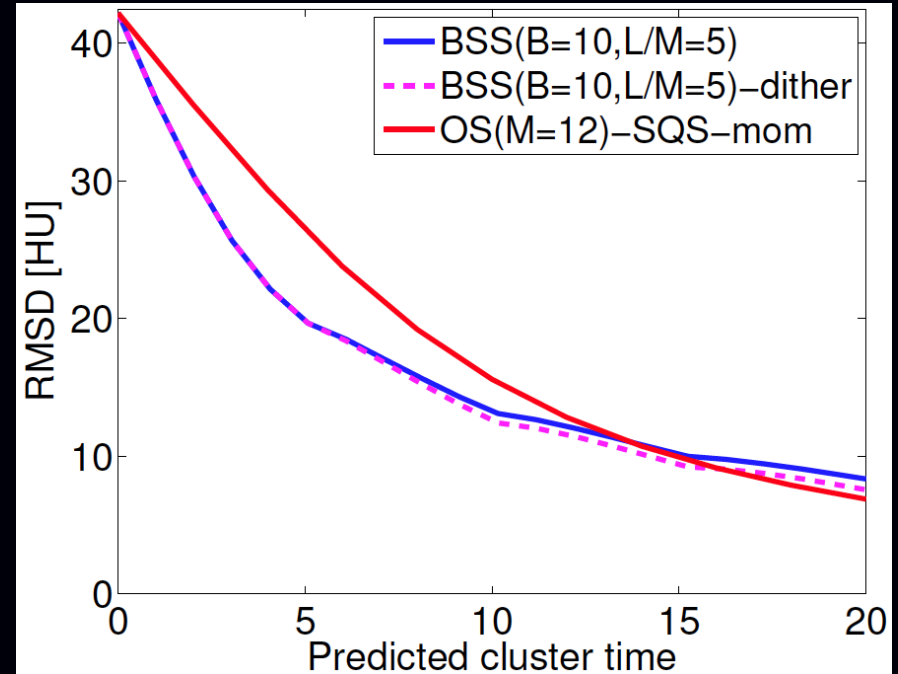
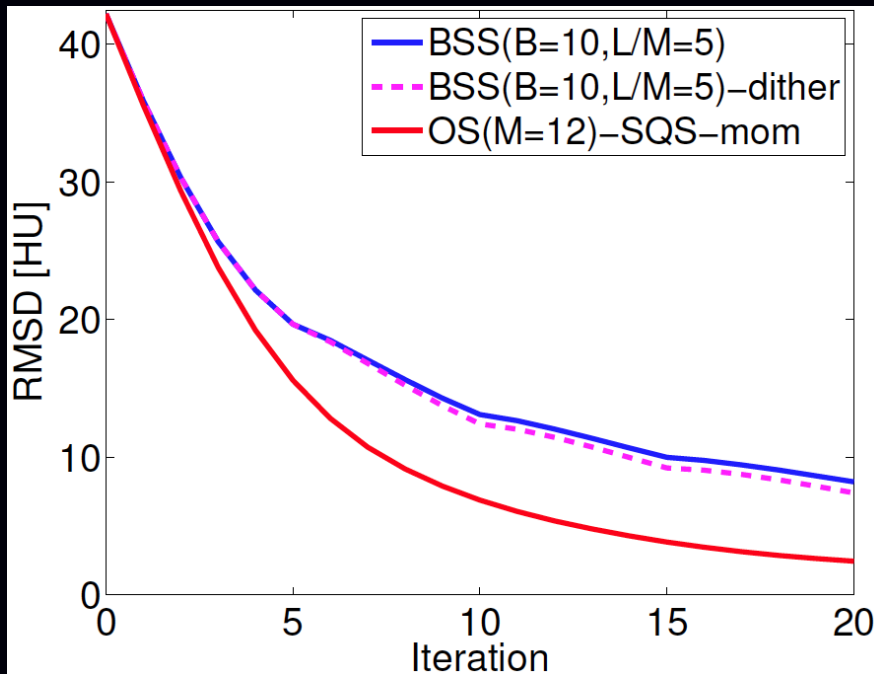
FBP initializer  $\mathbf{x}^{(0)}$



Converged  $\mathbf{x}^{(\infty)}$

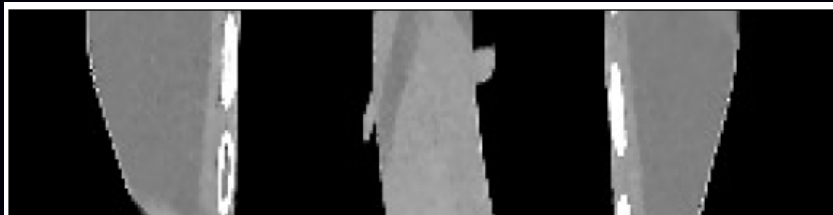


## BSS OS+OGM: rates



- Outer loop interrupts momentum  $\implies$  BSS is slower per iteration than OS+OGM
- Reduced communication reduces overall time

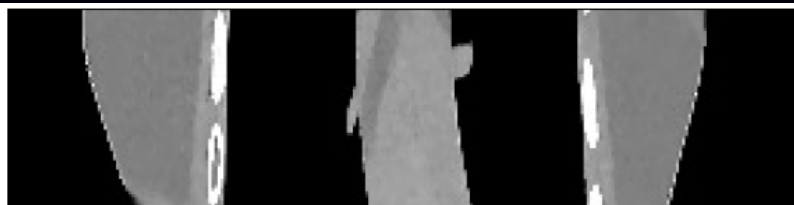
## BSS OS+OGM: images



(a)  $x^{(10)}$  of OS-SQS-mom( $M=12$ )



(b) Difference between (a) and  $\hat{x}$



(c)  $x^{(20)}$  of BSS( $B=10, M=12, L/M=5$ )



(d) Difference between (c) and  $\hat{x}$

- Comparable images
- Algorithm designed for distributed computation
- More results by Fully 3D conference in June...

# Duality approach for using GPU

- Data transfer between system RAM and GPU can be bottleneck
- Want to “hide” communication time by overlapping with computation

Algorithm synopsis:

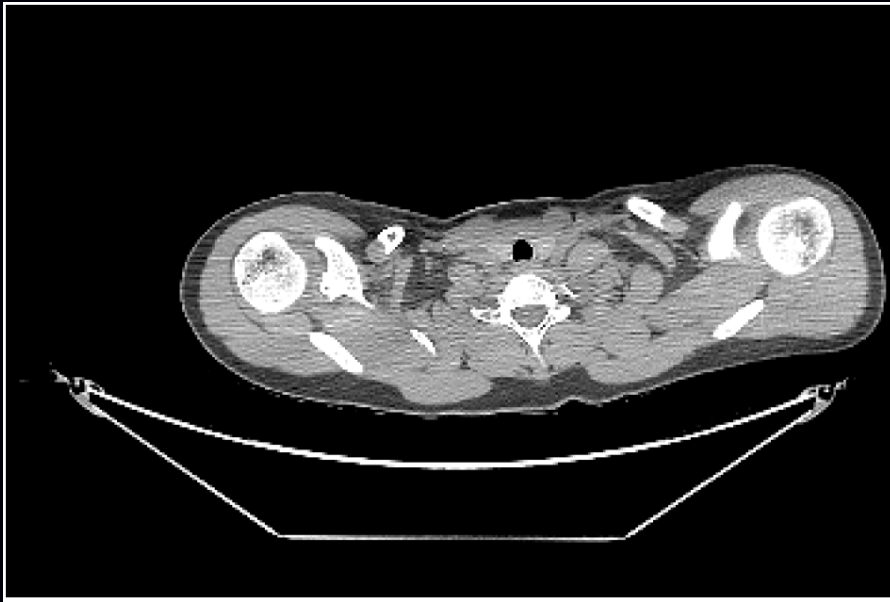
Madison McGaffin and JF; Fully 3D, 2015 (to appear)

- Write cost function  $\Psi(\mathbf{x})$  in terms of dual variables for data-fit and regularizer
- Alternate between updating several projection view dual variables and dual variables for one regularization direction
- Using dual variables “decouples” regularizer and data terms
- More details at Fully 3D ...

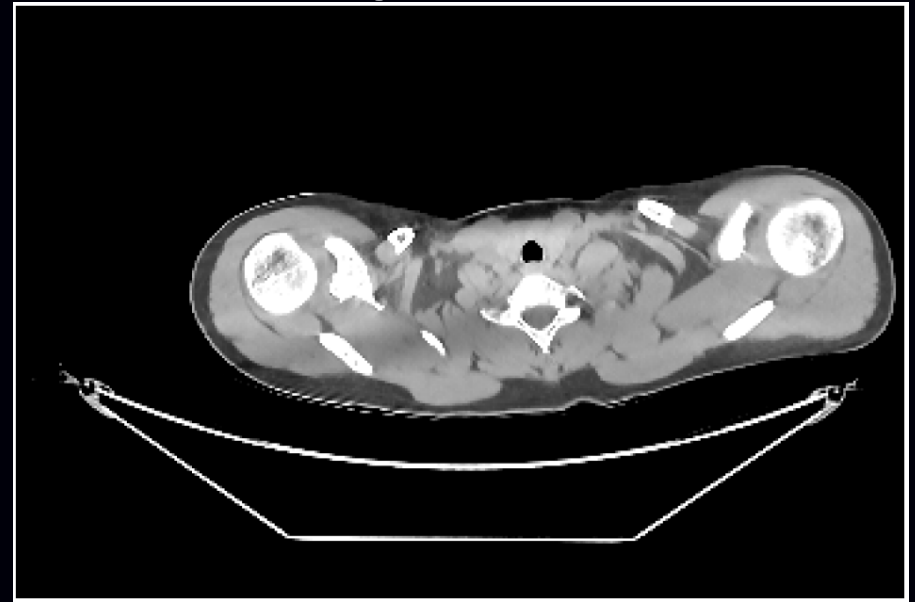
## Duality-GPU: data

- 3D cone-beam helical X-ray CT scan
- pitch 0.5
- image  $\mathbf{x}$ :  $512 \times 512 \times 109$  with 70 cm FOV and 0.625 mm slices
- sinogram :  $\mathbf{y}$  888 detectors  $\times$  32 rows  $\times$  7146 views
- OpenCL on aging NVIDIA GTX 480 GPU with 2.5 GB of memory

FBP initializer  $\mathbf{x}^{(0)}$

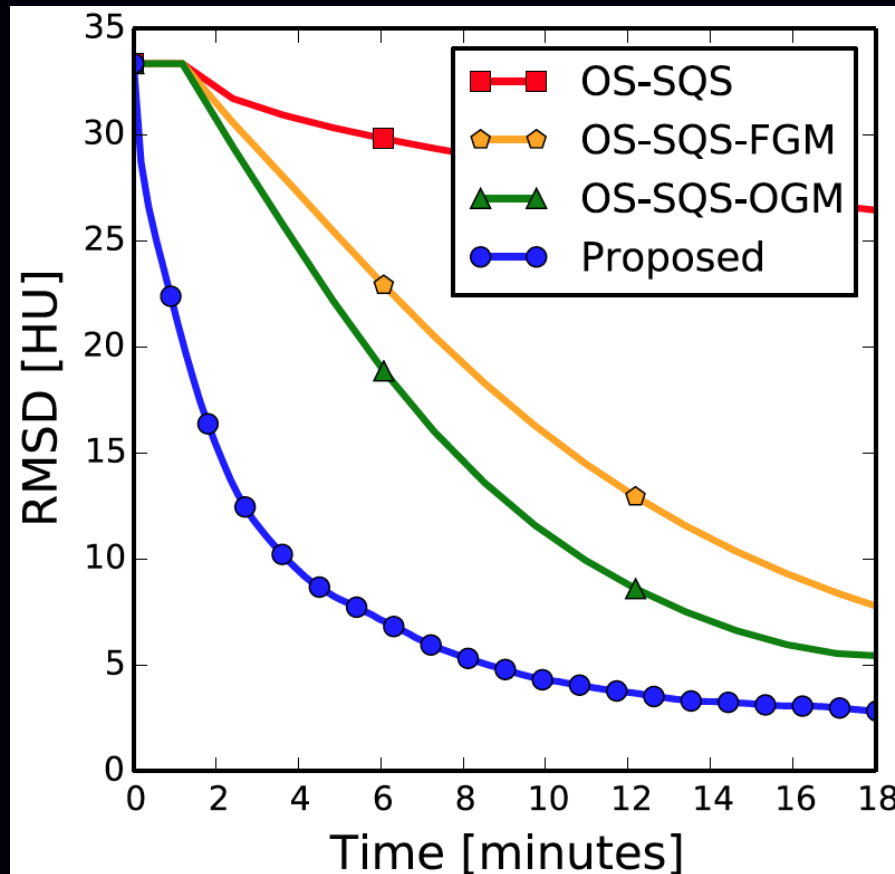


Converged  $\mathbf{x}^{(\infty)}$





## Duality-GPU: results



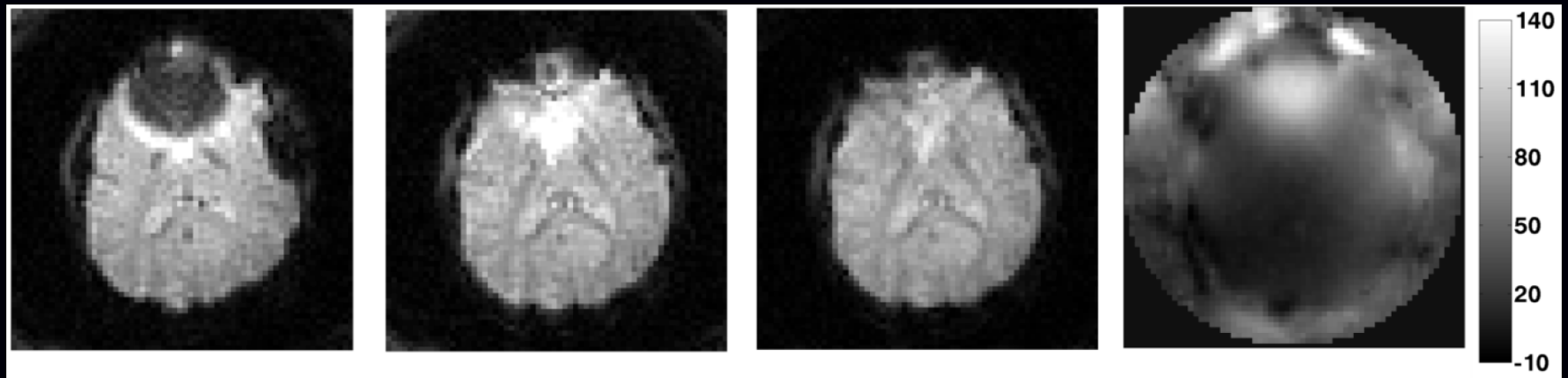
- Algorithm designed specifically for (single) GPU characteristics
- Future work:
  - combine with BSS for multiple nodes
  - multiple-GPU per-node extension
- More results by Fully 3D conference in June...

# **MRI image reconstruction**

# MRI: Why iterative reconstruction?

- Better physics modeling (e.g., field inhomogeneity)  $\implies$  reduced artifacts

Example: T2\*-weighted imaging Sutton *et al.*, IEEE T-MI, 2003



uncorrected

traditional

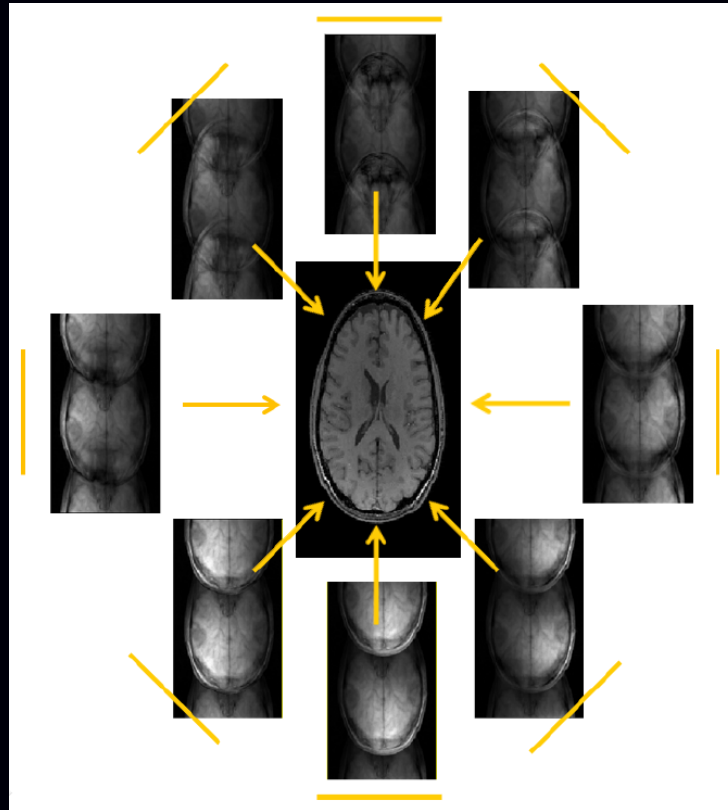
model-based

field map

- Reducing scan time (“under-sampling”)
  - Multiple receive coils
  - Object model assumptions (e.g., sparsity)

# Parallel MRI

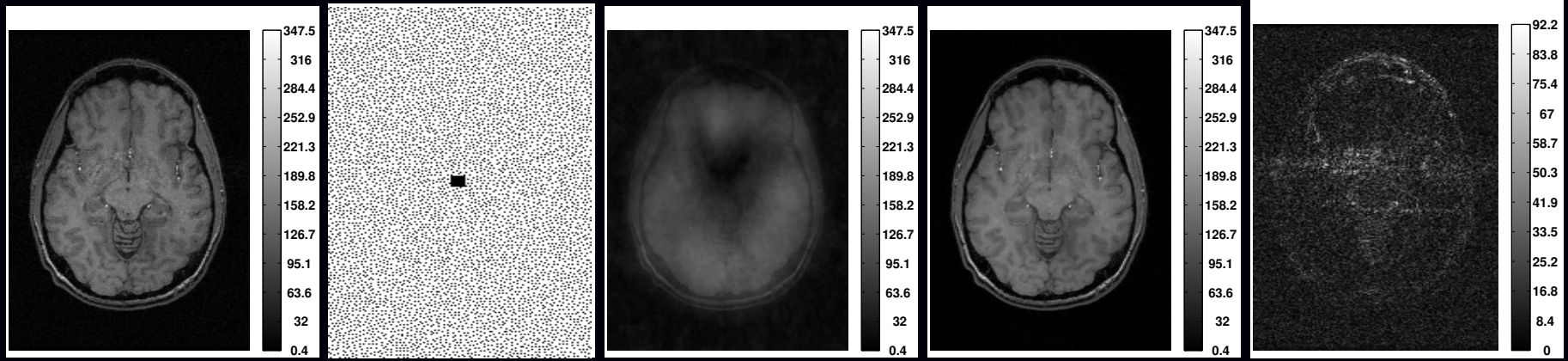
Undersampled Cartesian k-space, multiple receive coils, ...  
(Pruessmann *et al.*, MRM, Nov. 1999)



Compressed sensing parallel MRI  $\equiv$  further (random) under-sampling  
Lustig *et al.*, IEEE Sig. Proc. Mag., Mar. 2008

## 2.5D parallel MR image reconstruction

Example of “compressed sensing” MRI reconstruction:



- Fully sampled body coil image of human brain
- Poisson-disk-based k-space sampling, 16% sampling (acceleration 6.25)
- Square-root of sum-of-squares inverse FFT of zero-filled k-space data for 8 coils ( $144 \times 128$ )
- Regularized reconstruction  $\mathbf{x}^{(\infty)}$   
combined TV and  $\ell_1$  norm of two-level undecimated Haar wavelets
- Difference image magnitude

(Sathish Ramani & JF, IEEE T-MI, Mar. 2011)

# Model-based image reconstruction in parallel MRI

Regularized estimator:

$$\hat{\mathbf{x}} = \arg \min_{\mathbf{x}} \underbrace{\frac{1}{2} \|\mathbf{y} - \mathbf{F}\mathbf{S}\mathbf{x}\|_2^2}_{\text{data fit}} + \beta \underbrace{\|\mathbf{R}\mathbf{x}\|_p}_{\text{sparsity}}.$$

$\mathbf{F}$  is under-sampled DFT matrix (fat)

Features:

- coil sensitivity matrix  $\mathbf{S}$  is block diagonal (Pruessmann *et al.*, MRM, Nov. 1999)
- $\mathbf{F}'\mathbf{F}$  is circulant (for Cartesian sampling)

Complications:

- Data-fit Hessian  $\mathbf{S}'\mathbf{F}'\mathbf{F}\mathbf{S}$  is highly shift variant due to coil sensitivity maps
- Non-quadratic (edge-preserving) regularization  $\|\cdot\|_p$
- Non-smooth regularization  $\|\cdot\|_1$
- Complex quantities
- Large problem size (if 3D or dynamic or many coils)

## ISTA methods for parallel MRI

“Traditional” iterative soft thresholding algorithm (ISTA) for sparsity regularized problems uses (global) Lipschitz constant of data-fit term:

$$\nabla^2 \frac{1}{2} \|\mathbf{y} - \mathbf{F}\mathbf{S}\|_2^2 = \mathbf{S}'\mathbf{F}'\mathbf{F}\mathbf{S} \leq \mathbf{S}'\mathbf{S} \leq \lambda_{\max} \mathbf{I}, \quad \lambda_{\max} = \max_j [\mathbf{S}'\mathbf{S}]_{j,j}$$

$\lambda_{\max}$  is maximum sum-of-squares value of sensitivity maps; step size is  $1/\lambda_{\max}$

Augmented Lagrangian (AL) methods converge faster than ISTA, FISTA, MFISTA

**BARISTA**: B1-based, adaptive restart, iterative soft thresholding algorithms

For synthesis operator  $\mathbf{x} = \mathbf{Q}\mathbf{z}$  with  $\mathbf{z}$  sparse:

$$\nabla^2 \frac{1}{2} \|\mathbf{y} - \mathbf{F}\mathbf{S}\mathbf{Q}\|_2^2 = \mathbf{Q}'\mathbf{S}'\mathbf{F}'\mathbf{F}\mathbf{S}\mathbf{Q} \leq \mathbf{Q}'\mathbf{S}'\mathbf{S}\mathbf{Q} \leq \mathbf{D}$$

for a suitable diagonal matrix  $\mathbf{D}$ . (cf., SQS) (Muckley *et al.*, IEEE T-MI, Feb. 2015)

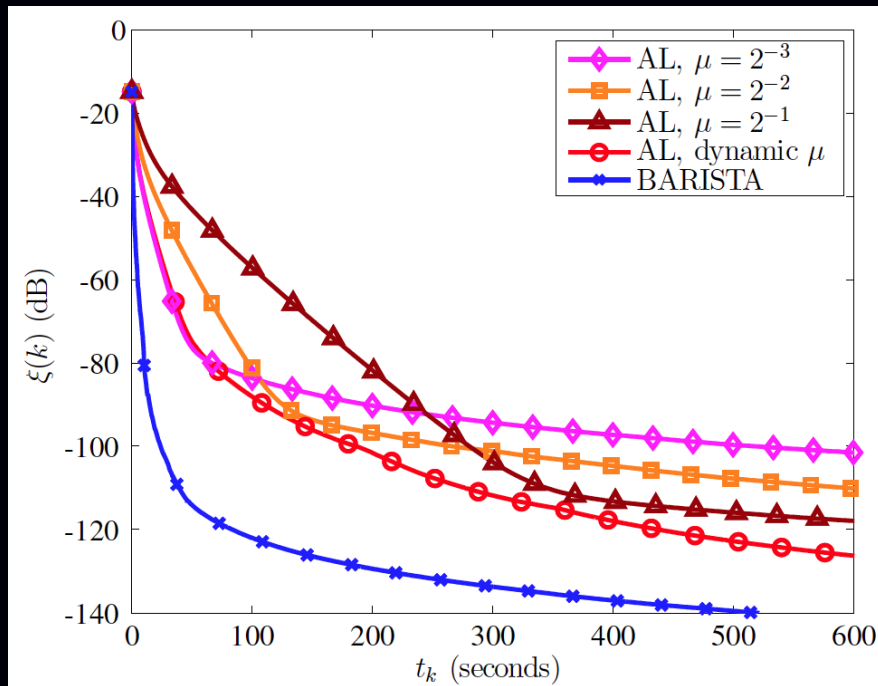
$\mathbf{D}^{-1}$  becomes voxel-dependent step size, akin to that in CT

Include momentum and adaptive restart of O'Donoghue and Candès (2014).

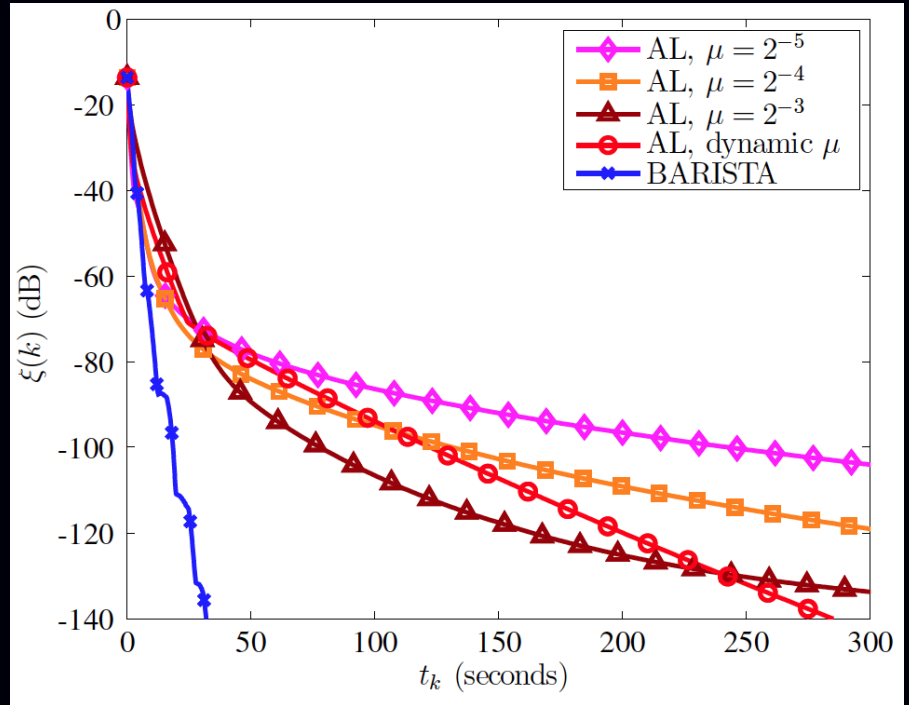
# BARISTA convergence rates

Example of “compressed sensing” MRI reconstruction:

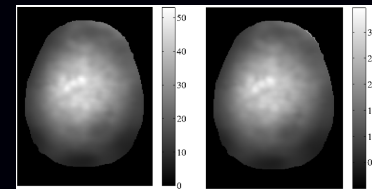
Total variation (TV) regularizer



Undecimated Haar Wavelets



Corresponding  $\mathbf{D}$  for each of the two cases:  
BARISTA requires no algorithm parameter tuning, unlike AL.





# Summary

Model-based image reconstruction can

- improve image quality for low-dose X-ray CT
- enable faster MRI scans via under-sampling

Computation time remains a significant challenge

Moore's law will not solve the problem

Algorithms designed for distributed computation are essential

# Bibliography

- [1] D. Kim and J. A. Fessler. Optimized first-order methods for smooth convex minimization. *Mathematical Programming*, 2014. Submitted.
- [2] D. Kim and J. A. Fessler. Optimized first-order methods for smooth convex minimization, 2014. arxiv 1406.5468.
- [3] D. Kim and J. A. Fessler. An optimized first-order method for image restoration. In *Proc. IEEE Intl. Conf. on Image Processing*, 2015. Submitted.
- [4] D. Kim, S. Ramani, and J. A. Fessler. Combining ordered subsets and momentum for accelerated X-ray CT image reconstruction. *IEEE Trans. Med. Imag.*, 34(1):167–78, January 2015.
- [5] D. Kim and J. A. Fessler. Distributed block-separable ordered subsets for helical X-ray CT image reconstruction. In *Proc. Intl. Mtg. on Fully 3D Image Recon. in Rad. and Nuc. Med*, 2015. To appear.
- [6] M. G. McGaffin and J. A. Fessler. Fast GPU-driven model-based X-ray CT image reconstruction via alternating dual updates. In *Proc. Intl. Mtg. on Fully 3D Image Recon. in Rad. and Nuc. Med*, 2015. To appear.
- [7] M. J. Muckley, D. C. Noll, and J. A. Fessler. Fast parallel MR image reconstruction via B1-based, adaptive restart, iterative soft thresholding algorithms (BARISTA). *IEEE Trans. Med. Imag.*, 34(2):578–88, February 2015.
- [8] D. E. Kuhl and R. Q. Edwards. Image separation radioisotope scanning. *Radiology*, 80(4):653–62, April 1963.
- [9] D. A. Chesler. Three-dimensional activity distribution from multiple positron scintigraphs. *J. Nuc. Med.*, 12(6):347–8, June 1971.
- [10] M. Goitein. Three-dimensional density reconstruction from a series of two-dimensional projections. *Nucl. Instr. Meth.*, 101(3):509–18, June 1972.
- [11] W. H. Richardson. Bayesian-based iterative method of image restoration. *J. Opt. Soc. Am.*, 62(1):55–9, January 1972.
- [12] L. Lucy. An iterative technique for the rectification of observed distributions. *The Astronomical Journal*, 79(6):745–54, June 1974.
- [13] A. J. Rockmore and A. Macovski. A maximum likelihood approach to emission image reconstruction from projections. *IEEE Trans. Nuc. Sci.*, 23:1428–32, 1976.
- [14] L. A. Shepp and Y. Vardi. Maximum likelihood reconstruction for emission tomography. *IEEE Trans. Med. Imag.*, 1(2):113–22, October 1982.
- [15] S. Geman and D. E. McClure. Bayesian image analysis: an application to single photon emission tomography. In *Proc. of Stat. Comp. Sect. of Amer. Stat. Assoc.*, pages 12–8, 1985.
- [16] H. M. Hudson and R. S. Larkin. Accelerated image reconstruction using ordered subsets of projection data. *IEEE Trans. Med. Imag.*, 13(4):601–9, December 1994.
- [17] J. Llacer, E. Veklerov, L. R. Baxter, S. T. Grafton, L. K. Griffeth, R. A. Hawkins, C. K. Hoh, J. C. Mazziotta, E. J. Hoffman, and C. E. Metz. Results of a clinical receiver operating characteristic study comparing filtered backprojection and maximum likelihood estimator images in FDG PET studies. *J. Nuc. Med.*, 34(7):1198–203, July 1993.
- [18] S. R. Meikle, B. F. Hutton, D. L. Bailey, P. K. Hooper, and M. J. Fulham. Accelerated EM reconstruction in total-body PET: potential for improving tumour detectability. *Phys. Med. Biol.*, 39(10):1689–794, October 1994.
- [19] G. Hounsfield. A method of apparatus for examination of a body by radiation such as x-ray or gamma radiation, 1972. US Patent 1283915. British patent 1283915, London.
- [20] R. Gordon, R. Bender, and G. T. Herman. Algebraic reconstruction techniques (ART) for the three-dimensional electron microscopy and

- X-ray photography. *J. Theor. Biol.*, 29(3):471–81, December 1970.
- [21] R. Gordon and G. T. Herman. Reconstruction of pictures from their projections. *Comm. ACM*, 14(12):759–68, December 1971.
  - [22] G. T. Herman, A. Lent, and S. W. Rowland. ART: mathematics and applications (a report on the mathematical foundations and on the applicability to real data of the algebraic reconstruction techniques). *J. Theor. Biol.*, 42(1):1–32, November 1973.
  - [23] R. Gordon. A tutorial on ART (algebraic reconstruction techniques). *IEEE Trans. Nuc. Sci.*, 21(3):78–93, June 1974.
  - [24] R. L. Kashyap and M. C. Mittal. Picture reconstruction from projections. *IEEE Trans. Comp.*, 24(9):915–23, September 1975.
  - [25] A. J. Rockmore and A. Macovski. A maximum likelihood approach to transmission image reconstruction from projections. *IEEE Trans. Nuc. Sci.*, 24(3):1929–35, June 1977.
  - [26] K. Lange and R. Carson. EM reconstruction algorithms for emission and transmission tomography. *J. Comp. Assisted Tomo.*, 8(2):306–16, April 1984.
  - [27] K. Sauer and C. Bouman. A local update strategy for iterative reconstruction from projections. *IEEE Trans. Sig. Proc.*, 41(2):534–48, February 1993.
  - [28] S. H. Manglos, G. M. Gagne, A. Krol, F. D. Thomas, and R. Narayanaswamy. Transmission maximum-likelihood reconstruction with ordered subsets for cone beam CT. *Phys. Med. Biol.*, 40(7):1225–41, July 1995.
  - [29] C. Kamphuis and F. J. Beekman. Accelerated iterative transmission CT reconstruction using an ordered subsets convex algorithm. *IEEE Trans. Med. Imag.*, 17(6):1001–5, December 1998.
  - [30] H. Erdoğan and J. A. Fessler. Ordered subsets algorithms for transmission tomography. *Phys. Med. Biol.*, 44(11):2835–51, November 1999.
  - [31] Y. Drori and M. Teboulle. Performance of first-order methods for smooth convex minimization: A novel approach. *Mathematical Programming*, 145(1-2):451–82, June 2014.
  - [32] Y. Nesterov. A method for unconstrained convex minimization problem with the rate of convergence  $O(1/k^2)$ . *Dokl. Akad. Nauk. USSR*, 269(3):543–7, 1983.
  - [33] Y. Nesterov. Smooth minimization of non-smooth functions. *Mathematical Programming*, 103(1):127–52, May 2005.
  - [34] A. B. Taylor, J. M. Hendrickx, and François Glineur. Smooth strongly convex interpolation and exact worst-case performance of first-order methods, 2015. arxiv 1502.05666.
  - [35] D. Kim and J. A. Fessler. Optimized momentum steps for accelerating X-ray CT ordered subsets image reconstruction. In *Proc. 3rd Intl. Mtg. on image formation in X-ray CT*, pages 103–6, 2014.
  - [36] J. M. Rosen, J. Wu, T. F. Wenisch, and J. A. Fessler. Iterative helical CT reconstruction in the cloud for ten dollars in five minutes. In *Proc. Intl. Mtg. on Fully 3D Image Recon. in Rad. and Nuc. Med*, pages 241–4, 2013.
  - [37] W. P. Segars, M. Mahesh, T. J. Beck, E. C. Frey, and B. M. W. Tsui. Realistic CT simulation using the 4D XCAT phantom. *Med. Phys.*, 35(8):3800–8, August 2008.
  - [38] B. P. Sutton, D. C. Noll, and J. A. Fessler. Fast, iterative image reconstruction for MRI in the presence of field inhomogeneities. *IEEE Trans. Med. Imag.*, 22(2):178–88, February 2003.
  - [39] K. P. Pruessmann, M. Weiger, M. B. Scheidegger, and P. Boesiger. SENSE: sensitivity encoding for fast MRI. *Mag. Res. Med.*, 42(5):952–62, November 1999.
  - [40] M. Lustig, D. L. Donoho, J. M. Santos, and J. M. Pauly. Compressed sensing MRI. *IEEE Sig. Proc. Mag.*, 25(2):72–82, March 2008.

- [41] S. Ramani and J. A. Fessler. Parallel MR image reconstruction using augmented Lagrangian methods. *IEEE Trans. Med. Imag.*, 30(3):694–706, March 2011.
- [42] B. O’Donoghue and E. Candès. Adaptive restart for accelerated gradient schemes. *Found. Computational Math.*, 2014.